Evaluation and Validation of Equivalent Circuit Photovoltaic Solar Cell Performance Models

Matthew T. Boyd

Sanford A. Klein
e-mail: klein@engr.wisc.edu

Douglas T. Reindl

Solar Energy Laboratory,
University of Wisconsin-Madison,
1500 Engineering Drive,
Madison, WI 53706

Brian P. Dougherty
National Institute of Standards and Technology,
100 Bureau Drive,
Gaithersburg, MD 20899

The "five-parameter model" is a performance model for photovoltaic solar cells that predicts the voltage and current output by representing the cells as an equivalent electrical circuit with radiation and temperature-dependent components. An important feature of the five-parameter model is that its parameters can be determined using data commonly provided by module manufacturers on their published datasheets. This paper documents the predictive capability of the five-parameter model and proposes modifications to improve its performance using approximately 30 days of field-measured meteorological and module data from a wide range of cell technologies, including monocrystalline, polycrystalline, amorphous silicon, and copper indium diselenide (CIS). The standard five-parameter model is capable of predicting the performance of monocrystalline and polycrystalline silicon modules within approximately 6% RMS but is slightly less accurate for a thin-film CIS and an amorphous silicon array. Errors for the amorphous technology are reduced to approximately 5% RMS by using input data obtained after the module underwent an initial degradation in output due to aging. The robustness and possible improvements to the five-parameter model were also evaluated. A sensitivity analysis of the five-parameter model shows that all model inputs that are difficult to determine and not provided by manufacturer datasheets such as the glazing material properties, the semiconductor band gap energy, and the ground reflectance may be represented by approximate values independent of the PV technology. Modifications to the five-parameter model tested during this research did not appreciably improve the overall model performance. Additional dependence introduced by a seven-parameter model had a less than 1% RMS effect on maximum power predictions for the amorphous technology and increased the modeling errors for this array 4% RMS at open-circuit conditions. Adding a current sink to the equivalent circuit to better model recombination currents had little effect on the model behavior. [DOI: 10.1115/1.4003584]

1 Introduction

The ability to predict the instantaneous power and annual energy output of photovoltaic (PV) solar panels is an integral part of system sizing, economic analysis, and electric power grid management. Several models already exist for predicting maximum power and current-voltage (*I-V*) relationships, but improvements may be possible by utilizing additional data recently provided by manufacturers. This paper reports on alternative formulations of the "five-parameter" equivalent circuit model using these additional manufacturer data. The five-parameter model provides accurate predictions for monocrystalline and polycrystalline cell technologies [1], but its ability to predict amorphous, multijunction, and other thin-film cell performance has not yet been established. This paper documents the performance of the five-parameter model for these PV technologies.

The electrical circuit models, such as the five-parameter model, represent solar cells as an equivalent electrical circuit with radiation and temperature-dependent components. The simplest of these equivalent circuits include only a radiation-dependent current source in parallel with a temperature-dependent diode, while more complex circuits include multiple diodes as well as series and parallel resistances. These equivalent circuit models are capable of predicting the electrical output at all points along the *I-V* curve.

Model parameters vary with the number of circuit components and their respective dependencies. As its name implies, the five-parameter model has five model parameters that are determined using only data available on PV manufacturer datasheets. Parameters in more complex models that have more circuit components can be determined using a nonlinear regression analysis [2–4] or a successive approximation [5] of multiple measured *I-V* curves.

The necessary inputs for electrical circuit models are the absorbed irradiance and cell temperature. The absorbed irradiance can be modeled by a number of radiation and cover models [6], while the cell temperature is either assumed equal to the backside panel temperature, which is measured, or approximated using empirical [7], semi-empirical [8,9], or theoretical [10,11] heat transfer models.

2 Measured Data

The PV module characterization data needed for the five-parameter model are measured at standard test conditions (STC) and provided on manufacturer datasheets; a description of these data is shown in Table 1.

The STCs for module performance are 1000 W/m^2 incident normal irradiance, 25 °C cell temperature, and a standard spectral distribution characteristic of a 1.5 air mass (AM). PV manufacturers report cell and module performance data at STC and oftentimes at other operating conditions on their datasheets; however, the characterization data used here were independently measured at the National Institute of Standards and Technology (NIST) in an effort to remove any measurement bias [12]. Characterization data measured at NIST for the six PV modules referenced in this research are provided in Table 2. The cell technologies of these modules include monocrystalline silicon (mono-Si), polycrystal-

Contributed by the Solar Energy Division of ASME for publication in the JOURNAL OF SOLAR ENERGY ENGINEERING. Manuscript received February 17, 2010; final manuscript received June 23, 2010; published online March 22, 2011. Assoc. Editor: Ignacio Tobías.

Table 1 Module characterization data needed for the five-parameter model

Datum	Unit	Description
I_{sc}	A	Current at short circuit
V_{oc}	V	Voltage at open circuit
I_{mp}	A	Current at maximum power
V_{mp}	V	Voltage at maximum power
$\alpha_{I_{sc}}$	A/°C	Temperature coefficient of short-circuit current
$\beta_{V_{oc}}$	V/°C	Temperature coefficient of open-circuit voltage

line silicon (poly-Si), tandem-junction amorphous silicon (2-a-Si), and copper indium diselenide (CIS). Table 2 also includes module characterization data for two of the modules at 200 W/m^2 and 25°C determined using linear regression of approximately 20 operating points nearest to these conditions.

2.1 Test Bed. Module, solar, and environmental data were measured by NIST in Gaithersburg, MD (39.17°N and 77.17°W). All modules were oriented vertically and south-facing, installed flush with the exterior building envelope within third floor modified window frames. The backsides of the six referenced modules were insulated with 100 mm of extruded polystyrene. Each module junction box was installed on the interior wall next to the module instead of on the backside of the module. This alternative placement was intended to reduce temperature gradients and allow for uniform insulation installation.

2.2 Module Measurements. All modules had one or more thermocouples centrally installed on their backside, with redundant thermocouples connected to a redundant data acquisition system; no spatial temperature measurements on the backsides of the modules were made. The mono-Si and poly-Si modules were custom made and had embedded thermocouples to more accurately measure the *cell temperature*. These cell temperature data show that the externally measured backside panel temperature was within ±1°C of the cell temperature at all operating conditions [12].

Module power leads were connected to a multi-tracer that regulated the voltage and kept the modules operating at maximum power. The multi-tracer sampled module current, voltage, power, and temperature at 5 s intervals and recorded the averages every 5 min. *I-V* curves were traced and logged every 5 min from short circuit ($V=0$) to open circuit ($I=0$). Module temperature, ambient temperature, and plane-of-array (POA) irradiance data measured by a thermopile-based pyranometer were recorded immediately before and after each *I-V* trace.

Table 3 Meteorological measurements and the corresponding instruments

Measurement	Instrument	Location
Beam normal irradiance (G_{bn})	Pyrheliometer	Rooftop tracking
Diffuse horizontal irradiance (G_d)	Shaded disk with thermopile-based pyranometer	
Global horizontal irradiance (G)	Thermopile-based pyranometer	Rooftop fixed
Plane of array global irradiance (G_T)		Plane-of-array fixed

2.3 Meteorological Measurements. In addition to the POA measurements—which included wind speed and wind direction—data were also recorded at a meteorological station located on the rooftop of the same building as the installed PV modules. A summary of the solar irradiance measurements and the corresponding

Table 2 Module specification and measured characteristic data

Module ID	A	B	C	D	F	H
Cell type	Monocrystalline	Polycrystalline			2-a-Si	CIS
Glazing material	Glass	Glass	ETFE	PVDF	Glass	Glass
I_{sc} [a] (A)	4.37	4.81	5.05	5.00	0.729	2.76
V_{oc} [a] (V)	42.93	42.73	42.77	42.91	99.56	23.66
I_{mp} [a] (A)	3.96	4.28	4.61	4.48	0.612	2.39
V_{mp} [a] (V)	33.68	34.17	33.45	34.32	76.51	16.18
P_{mp} [a] (W)	133.4	146.4	154.2	153.7	46.82	38.67
$\alpha_{I_{sc}}$ (A/°C)	0.00175	0.00384	0.00360	0.00339	0.00060	−0.00001
$\beta_{V_{oc}}$ (V/°C)	−0.152	−0.137	−0.131	−0.132	−0.412	−0.0916
$\gamma_{P_{mp}}$ (%/°C)	−0.495	−0.396	−0.398	−0.390	−0.355	−0.422
$\alpha_{I_{mp}}$ (%/°C)	−0.0390	0.0246	0.0185	0.0256	0.0997	−0.0533
$\beta_{V_{mp}}$ (%/°C)	−0.456	−0.420	−0.416	−0.415	−0.455	−0.369
$I_{mp,200}$ [b] (A)	0.86	–	–	–	0.115	–
$V_{mp,200}$ [b] (V)	33.3	–	–	–	65.5	–
NOCT (°C)	43.7	46.0	39.5	39.9	40.7	41.8
Total cell area (m^2)	1.020	1.134	1.134	1.134	1.487	1.451
Coverage area (m^2)	1.160	1.167	1.168	1.168	1.487	1.451
Glazing thickness (mm)	6	6	0.05	0.05	3	3
Cells in series	72	72	72	72	68	42
Parallel series strings	1	1	1	1	1	1
Modules in series	1	1	1	1	1	1
Modules in parallel	1	1	1	1	2	4

[a]As evaluated at STC.
[b]Representative of field conditions where the measured incident irradiance is approximately 200 W/m^2 and the PV module temperature is approximately 25°C.
Note: The following uncertainty values represent the expanded uncertainty using a coverage value of 2: $I_{sc}=\pm 1.7\%$, $V_{oc}=\pm 1.1\%$, $I_{mp}=\pm 1.6\%$, $V_{mp}=\pm 1.4\%$, and $P_{mp}=\pm 2.1\%$.

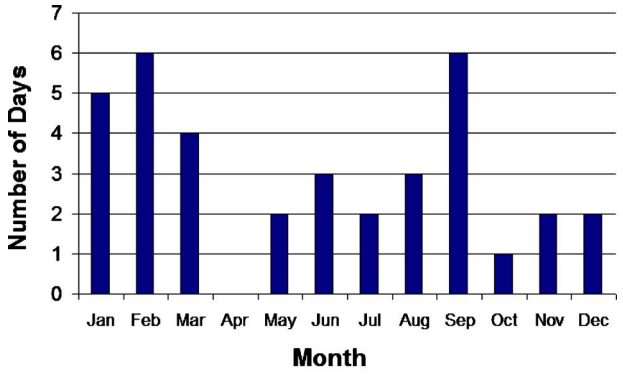

Fig. 1 Distribution of days of data selected for the clear days 9:30–4 EST data set

instruments is given in Table 3. Of the available field data, only the instantaneous meteorological measurements recorded at 5 min intervals were used for this PV model evaluation effort.

2.4 Compiled Data Sets. Two data sets were compiled from the entire database for use in validating the equivalent circuit PV performance models. One data set, named "clear days 9:30–4 EST," contains data from 36 of the clearest days dispersed throughout the year-long data acquisition period, with the number of days included from each month shown in Fig. 1. No days were selected from April because diffuse data measurements were not available during that month. Clear, irradiance-stable days were chosen to minimize any transient effects in the modules and measurement instruments. These clear day data span from 09:30 to 16:00 EST to avoid periods of time when one or more of the building-integrated PV modules would experience shading.

The second compiled data set, named "January–unshaded periods," contains data from January at times of no module shading. These data result in lower uncertainty in the calculation of absorbed irradiance because they occur at lower incidence angles on a vertical surface based on the sun's location in January. This data set also contains much more diffuse and low irradiance data, as shown by the histograms of incident POA irradiance in Fig. 2.

3 Radiation Model

3.1 HDKR Model. Radiation models calculate absorbed irradiance using some or all beam, diffuse, and ground reflected irradiance components, associated incidence angles, and glazing optical properties. Examples of such models are the Liu and Jordan isotropic sky, HDKR,[1] and Perez models [6]. A study of these radiation models [13] comparing modeled to measured irradiance showed that the Perez model was the most accurate, with the HDKR model following by about 1% root-mean-square error (RMSE) and 0.3% mean bias error (MBE). The HDKR model is used for this research because it has a much simpler implementation compared to the Perez model. The HDKR model for absorbed irradiance is shown in Eqs. (1)–(6), where the subscripts b, d, and g stand for beam, diffuse, and ground reflected, respectively. The ground reflectivity (ρ_g) is assumed to be 0.1 [14] because much of the ground in the module's field of view is asphalt.

$$S_{T,\mathrm{HDKR}} = (G_b + G_d A_i) R_b (\tau\alpha)_b + G_d (1 - A_i)(\tau\alpha)_d \left(\frac{1+\cos\beta}{2}\right)\left[1 + f\sin^3\left(\frac{\beta}{2}\right)\right] + G\rho_g (\tau\alpha)_g \left(\frac{1-\cos\beta}{2}\right) \quad (1)$$

$$A_i = \frac{G_{b,n}}{G_{on}} \quad (2)$$

$$f = \sqrt{\frac{G_b}{G}} \quad (3)$$

$$G_b = G_{b,n}\cos\theta_b \quad (4)$$

$$G = G_b + G_d \quad (5)$$

$$R_b = \frac{\cos(\phi-\beta)\cos\delta_{\mathrm{dec}}\cos\omega + \sin(\phi-\beta)\sin\delta_{\mathrm{dec}}}{\cos\phi\cos\delta_{\mathrm{dec}}\cos\omega + \sin\phi\sin\delta_{\mathrm{dec}}} \quad (6)$$

3.2 Transmittance-Absorptance Product. The multiple layers of PV module glazings have been shown to be well represented by a single air-glazing interface [6]. The optical effects of this interface are characterized by the transmittance-absorptance ($\tau\alpha$) product, which represents the fraction of the irradiance transmitted through the glazing and absorbed by the semiconductor. The ($\tau\alpha$) for a photovoltaic cell glazing is given in Eq. (7), with Snell's law (Eq. (8)) used to calculate the angle of refraction.

$$\tau\alpha(\theta) = e^{-(KL/\cos\theta_r)}\left[1 - \frac{1}{2}\left(\frac{\sin^2(\theta_r-\theta)}{\sin^2(\theta_r+\theta)} + \frac{\tan^2(\theta_r-\theta)}{\tan^2(\theta_r+\theta)}\right)\right] \quad (7)$$

$$n_{\mathrm{air}}\sin\theta = n_{\mathrm{glaz}}\sin\theta_r \quad (8)$$

The ($\tau\alpha$) product is a function of the incidence angle (θ), the refractive index of the air (n_{air}), the glazing thickness (L), the extinction coefficient (K), and the refractive index (n_{glaz}). The module glazings present in this analysis and their respective material property values are given in Table 4. Glass glazings are used on all the modules except for two of the three poly-Si modules; one has an ethylene tetrafluoroethylene (ETFE) and the other has

[1]Named after the collective work of Hay, Davies, Klucher, and Reindl.

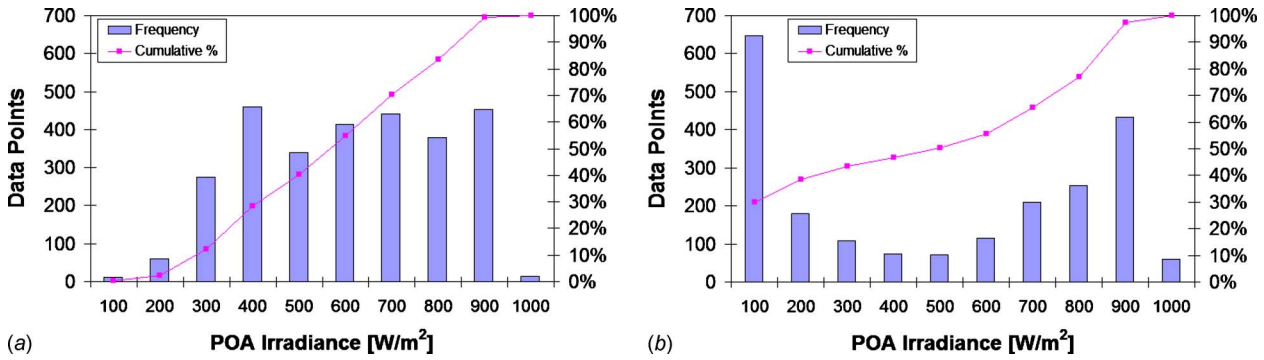

Fig. 2 Histograms of the (*a*) clear days 9:30–4 EST and (*b*) January–unshaded periods data sets used for model validation

Table 4 Module glazing material properties

Glazing material	$L \times 10^3$ (m)	K [a] (m^{-1})	n_{glaz}
Glass	3 and 6	4	1.526
ETFE	0.05	4	1.4
PVDF	0.05	4	1.42

[a]Values are estimates.

a polyvinylidene fluoride (PVDF) polymer glazing.

The extinction coefficient, K, quantifies the absorption losses of the glazing. Glass has an extinction coefficient ranging from 4 m^{-1} for "water white" glass to 32 m^{-1} for high iron oxide glass [6]. It is assumed that the glass glazings are water white and that the polymer (ETFE and PVDF) glazings have extinction coefficient values in between the values for water white and high iron oxide glass. In this range of extinction coefficients, using the manufacturer provided glazing thickness of 50 μm and refractive index of approximately 1.4 [15,16], $(\tau\alpha)$ changes by only -0.23% [17]. Therefore, an extinction coefficient of 4 is used for both the polymer glazings as specific measured values for the as-installed glazings are not known.

3.3 POA Correction Factor. The measured POA data are not directly used because all three irradiance components needed to estimate transmittance effects cannot be separated from this single measured POA value. The POA data were instead used to correct the HDKR radiation model estimates. The total irradiance on the vertical surface estimated using the HDKR model should equal the POA irradiance measurement when transmittance and absorptance effects are omitted. A correction factor, R, is defined to be the ratio of the measured POA irradiance to the modeled POA irradiance as defined in Eq. (9). This correction factor is then used to modify the calculated irradiance absorbed by the module, as indicated in Eq. (10). The effect of the correction factor is shown in Sec. 5.

$$R = \frac{G_{T,\mathrm{POA}}}{G_{T,\mathrm{HDKR}}} \tag{9}$$

$$S_{T,\mathrm{HDKR},c} = S_{T,\mathrm{HDKR}} \cdot R \tag{10}$$

4 Five-Parameter Model

4.1 Equivalent Circuit. The five-parameter PV performance model is derived from an equivalent circuit of a solar cell, which consists of a current source, a diode, and two resistors, as shown in Fig. 3.

The current source (I_L) represents charge carrier generation in the semiconductor layer of the PV cell caused by incident radiation. The shunt diode represents recombination of these charge carriers at a forward-bias voltage ($V+I\cdot R_s$). The shunt resistor (R_{sh}) signifies high-current paths through the semiconductor along mechanical defects and material dislocations [18]. The series resistor (R_s) embodies series resistance in the outer semiconductor regions, primarily at the interface of the semiconductor and the metal contacts [18].

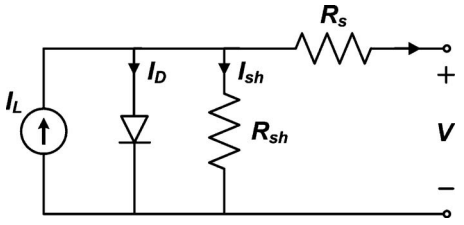

Fig. 3 Equivalent circuit of a photovoltaic solar cell used in the five-parameter model

A current balance at a point to the left of R_s as shown in Fig. 3 results in Eq. (11). Substituting in Ohm's law and the Shockley diode equation for the currents through the resistors and diode, respectively, yields the model characteristic equation, given by Eq. (12). The variable I_o is the reverse-bias saturation current and a is the modified ideality factor, defined by Eq. (13), where N_s is the number of solar cells in series, n is the diode ideality factor, k is Boltzmann's constant, T is the cell temperature, and q is the charge of an electron.

$$I = I_L - I_D - I_{\mathrm{sh}} \tag{11}$$

$$I(V) = I_L - I_o(e^{(V+IR_s)/a} - 1) - \frac{V + IR_s}{R_{\mathrm{sh}}} \tag{12}$$

$$a \equiv \frac{N_s n k T}{q} \tag{13}$$

4.2 Model Parameter Calculation. The characteristic equation of the equivalent circuit contains five independent parameters, hence the name *five-parameter model*. These parameters can be determined analytically using only the measurements at STC that are available on manufacturer datasheets: current at maximum power (I_{mp}), voltage at maximum power (V_{mp}), short-circuit current (I_{sc}), open-circuit voltage (V_{oc}), and temperature coefficients of short-circuit current ($\alpha_{I_{\mathrm{sc}}}$) and open-circuit voltage ($\beta_{V_{\mathrm{oc}}}$). The methodology to determine the model parameters involves first constraining the characteristic equation at short-circuit, open-circuit, and maximum power conditions, as shown in Eqs. (14)–(16), respectively. This results in three equations and five unknowns.

$$I_{\mathrm{sc}}|_{\mathrm{ref}} = \left[I_L - I_o(e^{I_{\mathrm{sc}}R_s/a} - 1) - \frac{I_{\mathrm{sc}}R_s}{R_{\mathrm{sh}}} \right]_{\mathrm{ref}} \tag{14}$$

$$0 = \left[I_L - I_o[e^{V_{\mathrm{oc}}/a} - 1] - \frac{V_{\mathrm{oc}}}{R_{\mathrm{sh}}} \right]_{\mathrm{ref}} \tag{15}$$

$$I_{\mathrm{mp}}|_{\mathrm{ref}} = \left[I_L - I_o(e^{(V_{\mathrm{mp}}+I_{\mathrm{mp}}R_s)/a} - 1) - \frac{V_{\mathrm{mp}} + I_{\mathrm{mp}}R_s}{R_{\mathrm{sh}}} \right]_{\mathrm{ref}} \tag{16}$$

The second step in the parameter solving methodology is to constrain the derivative of the product of the characteristic equation for the current and the voltage (which is the power) to zero at maximum power, as shown in Eq. (17). This equation along with the previous three result in four equations and five unknowns.

$$0 = \left[I_{\mathrm{mp}} + V_{\mathrm{mp}} \left(\frac{\frac{-I_o}{a} e^{(V_{\mathrm{mp}}+I_{\mathrm{mp}}R_s)/a} - \frac{1}{R_{\mathrm{sh}}}}{1 + \frac{I_o R_s}{a} e^{(V_{\mathrm{mp}}+I_{\mathrm{mp}}R_s)/a} + \frac{R_s}{R_{\mathrm{sh}}}} \right) \right]_{\mathrm{ref}} \tag{17}$$

The last step in the methodology is to use the known value and definition of $\beta_{V_{\mathrm{oc}}}$ assuming linearity (Eq. (18)) and to solve for the characteristic equation evaluated at the open-circuit condition at a non-reference temperature, as shown in Eq. (19). The temperature at which this equation is evaluated has little observed effect on the parameter solution, with a ΔT of 10 K assumed. To solve this additional equation, the temperature dependence of each of the parameters must be known. The dependencies determined in Ref. [1], given by Eqs. (20)–(24), are used. A linear temperature dependence is assumed for the material band gap energy (E_g) [19], and it is calculated using the reference value and temperature coefficient for silicon. A value of unity is used for the air mass modifier (M/M_{ref}) [1], and the equations are solved at the reference irradiance ($S=S_{\mathrm{ref}}$). Equations (18)–(24) result in seven

Table 5 Calculated input parameters for the five-parameter model using STC data

Module	a_{ref} (V)	$I_{L,\text{ref}}$ (A)	$I_{o,\text{ref}}$ (A)	$R_{s,\text{ref}}$ (Ω)	$R_{\text{sh,ref}}$ (Ω)
Mono-Si	1.77	4.40	1.19×10^{-9}	1.04	182
Poly-Si (glass)	1.68	4.85	4.04×10^{-11}	0.817	109
Poly-Si (ETFE)	1.64	5.08	2.30×10^{-11}	0.970	175
Poly-Si (PVDF)	1.65	5.04	2.29×10^{-11}	0.804	115
2-a-Si	4.48	0.742	1.41×10^{-10}	16.8	927
CIS	1.02	2.82	2.10×10^{-10}	2.05	93.5

equations and six additional unknowns, yielding closure for a total of 11 equations and 11 unknowns.

$$\beta_{V_{\text{oc}}} = \frac{V_{\text{oc}} - V_{\text{oc,ref}}}{T - T_{\text{ref}}} \tag{18}$$

$$0 = \left[I_L - I_o(e^{V_{\text{oc}}/a} - 1) - \frac{V_{\text{oc}}}{R_{\text{sh}}} \right]_{T=T_{\text{ref}}+\Delta T} \tag{19}$$

$$a = a_{\text{ref}} \frac{T}{T_{\text{ref}}} \tag{20}$$

$$I_L = \frac{S}{S_{\text{ref}}} \frac{M}{M_{\text{ref}}} [I_{L,\text{ref}} + \alpha_{I_{\text{sc}}}(T - T_{\text{ref}})] \tag{21}$$

$$I_o = I_{o,\text{ref}} \left(\frac{T}{T_{\text{ref}}} \right)^3 \exp\left[\frac{1}{k} \left(\left. \frac{E_g}{T} \right|_{T_{\text{ref}}} - \frac{E_g}{T} \right) \right] \tag{22}$$

$$R_{\text{sh}} = \frac{S_{\text{ref}}}{S} R_{\text{sh,ref}} \tag{23}$$

$$R_s = R_{s,\text{ref}} \tag{24}$$

There is no analytical solution to these highly nonlinear coupled equations, so they are solved numerically using the software program EES [20]. The calculated parameters for the modules included in this research are provided in Table 5.

4.3 Effect of Parameters on *I-V* Curve Shape. The effect of each of the five parameters on the behavior of the *I-V* curve is shown in Fig. 4. The model is calculated for a 2-a-Si module at an absorbed irradiance and cell temperature near the average of the corresponding yearly operating conditions for this location, 500 W/m^2 and 35 °C. The effect of each parameter on the *I-V* curve is similar for all modules and operating conditions. The bold *I-V* curve in each of these plots is the result of using parameters calculated from STC data, while the other two are the result of adjusting one specified parameter above and below the original value. These figures show that both a and I_o adjust the predicted voltage at all points on the *I-V* curve and I_L adjusts the predicted current. R_s and R_{sh} have a more localized influence around the maximum power point; R_s adjusts the maximum power voltage and R_{sh} adjusts the maximum power current.

5 Model Validation

5.1 Error Statistics. The two compiled data sets measured at NIST are used to validate the five-parameter model and its variations. Although the data sets include entire *I-V* curves for comparison with the model, only the operating points at short-circuit (I_{sc}), open-circuit (V_{oc}), and maximum power ($I_{\text{mp}}, V_{\text{mp}}, P_{\text{mp}}$) were compared, which simplifies the data processing and results. Statistics employed to quantify the model's agreement to the measured data at these five operating points are the root-mean-square error (RMSE), mean bias error (MBE), and mean absolute error (MAE), normalized as shown in Eqs. (25)–(27), where y is the modeled value, x is the measured value, and n is the total number of measured values.

$$\text{RMSE} = \left[\frac{1}{n} \sum_{i=1}^{n} (y_i - x_i)^2 \right]^{1/2} \div \left[\frac{1}{n} \sum_{i=1}^{n} x_i \right] \times 100\% \tag{25}$$

$$\text{MBE} = \left[\frac{1}{n} \sum_{i=1}^{n} (y_i - x_i) \right] \div \left[\frac{1}{n} \sum_{i=1}^{n} x_i \right] \times 100\% \tag{26}$$

$$\text{MAE} = \left[\frac{1}{n} \sum_{i=1}^{n} |y_i - x_i| \right] \div \left[\frac{1}{n} \sum_{i=1}^{n} x_i \right] \times 100\% \tag{27}$$

5.2 Effect of POA Correction Factor. The POA correction factor R, defined in Eq. (9), significantly reduces the modeling errors for all of the test modules. As one example, the differences between the five-parameter model and measured data for the mono-Si module are shown in Fig. 5 for the clear days 9:30–4 EST and January–unshaded periods data sets. The variables compared include short-circuit current, open-circuit voltage, maximum power, and current and voltage at maximum power. The POA correction factor is therefore used for all validations.

5.3 Validation Using Model Parameters Calculated From STC Data. Modeling errors are calculated for each array using parameters derived from STC data and using the POA correction factor. Statistical modeling errors are shown in Fig. 6. The results in Figs. 6(*a*)–6(*d*) show that the mono-Si and poly-Si modules are well represented by the five-parameter model, but there are significantly larger errors for the 2-a-Si and CIS arrays. The model exhibits large voltage bias errors for the 2-a-Si array at both open circuit and maximum power, which results in large corresponding RMS errors. The large voltage RMS errors for the CIS array have a comparatively lower corresponding bias error (MBE), which indicates more scatter. Additional detail is provided in Ref. [17].

5.4 Aging Effects of Amorphous Silicon. Five different sets of STC data for the 2-a-Si modules were measured when the modules had progressively larger amounts of cumulative lifetime exposure to solar irradiance. Three sets of STC data were measured from identical control modules within 1 month of initial solar exposure. Approximately 20 months later, two additional sets of STC data were measured from one of the installed amorphous silicon modules. These five sets of STC data and the corresponding exposures are listed in Table 6. The STC data values are all shown to decrease relative to the earliest measured set. The calculated model parameters for each of these five data sets are given in Table 7.

The earliest 2-a-Si STC data, measured after 9 days of solar exposure, were used to determine the model parameters for the five-parameter modeling error results shown in Fig. 6. These parameters, calculated from higher STC values, led the model to overestimate module performance after the degradation period. The 2-a-Si modeling errors for the clear days 9:30–4 EST data set using parameters calculated from each of the four additional STC data sets are shown in Fig. 7. The modeling errors are shown to be significantly lower when using parameters calculated from data obtained from aged modules because they are more representative of the module performance following the degradation period. Subsequent model validations use STC data measured after the module has reached stable performance, in this case after 631 days of solar exposure.

6 Sensitivity Analysis

A sensitivity analysis of the five-parameter model enables the determination of acceptable tolerances for the model inputs and identifies which inputs most significantly affect model predictions. Fifteen constant model inputs expected to have significant uncer-

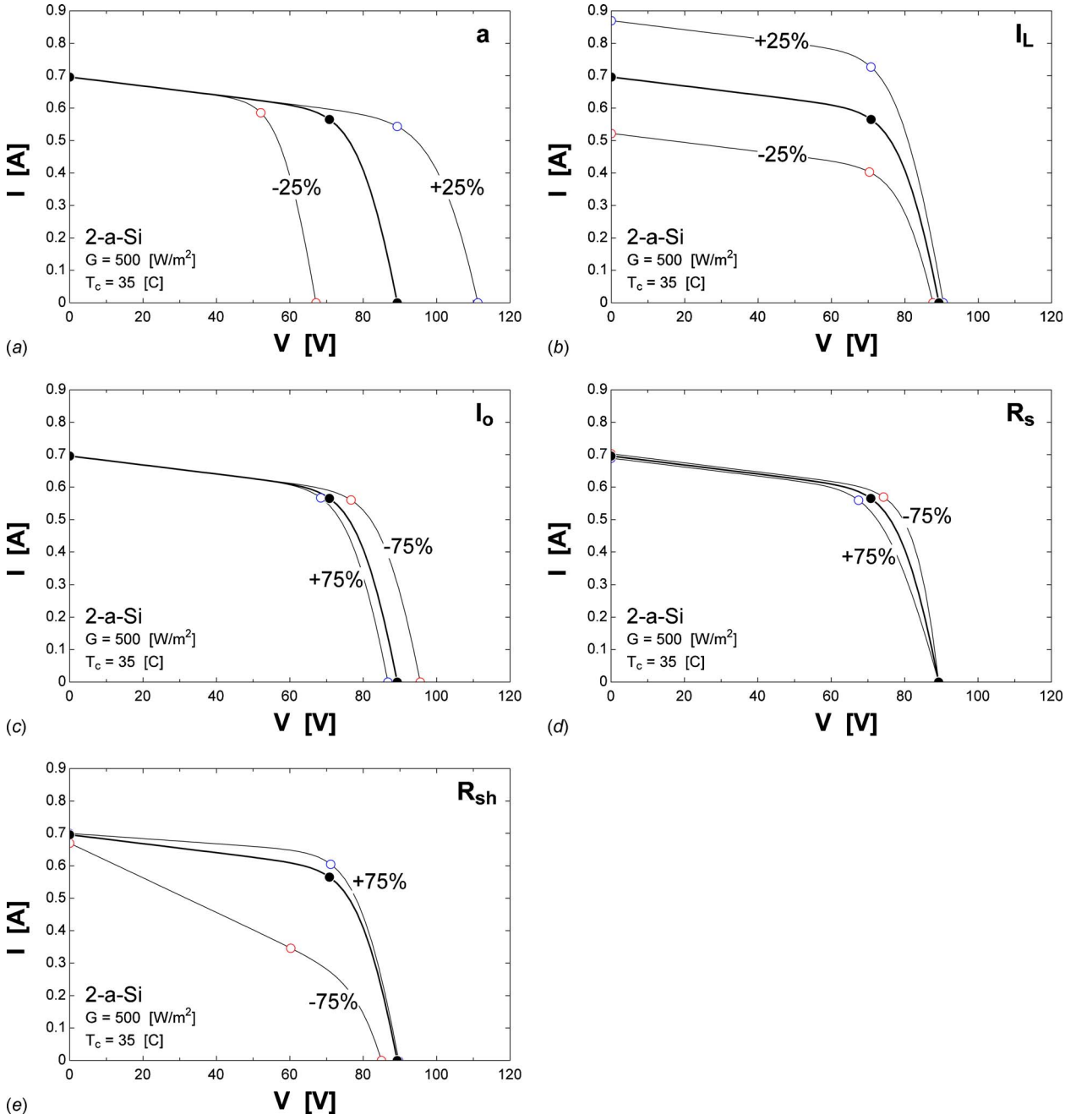

Fig. 4 Effect of the five parameters in the five-parameter model on the behavior of the modeled *I-V* curve

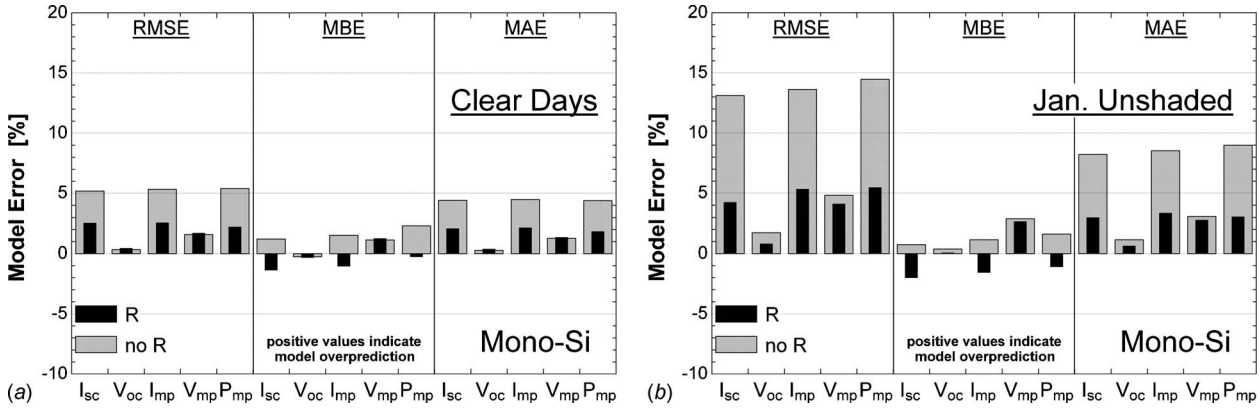

Fig. 5 Effect of the POA correction factor *R* on the five-parameter modeling errors for the mono-Si module for two different data sets

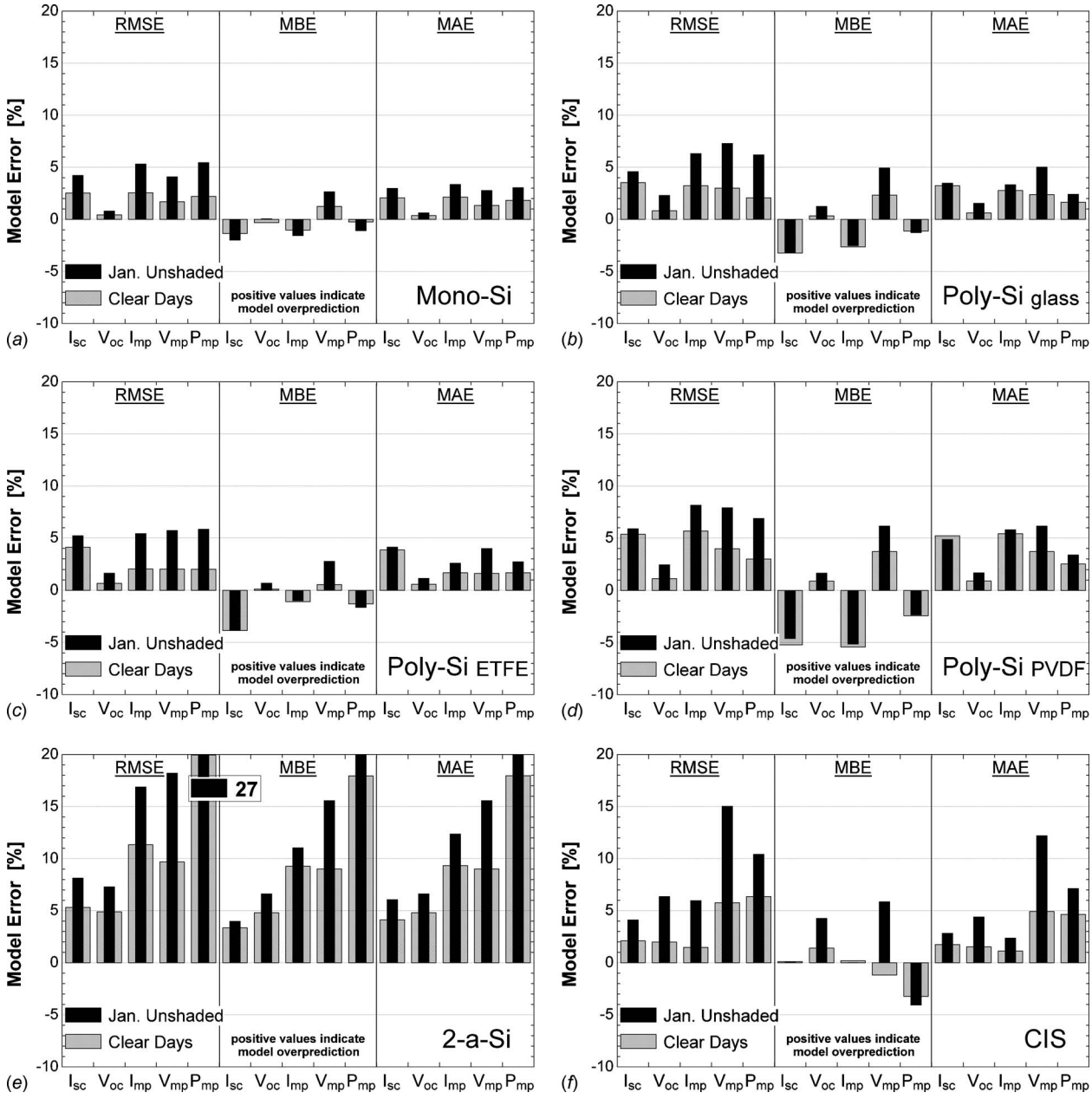

Fig. 6 Statistical modeling errors of the five-parameter model for the six backside insulated arrays using two different data sets ((*a*) mono-Si, (*b*) poly-Si (glass glazing), (*c*) poly-Si (ETFE glazing), (*d*) poly-Si (PVDF glazing), (*e*) 2-a-Si, and (*f*) CIS)

tainty and a strong effect on the model performance are included in the analysis. This analysis is performed by adjusting one variable at a time around the base value and by calculating the RMSEs between the model predictions and measured values. The analysis used data measured from the mono-Si module in the clear days 9:30–4 EST data set.

Table 6 STC data measured from the 2-a-Si technology with progressively longer periods of cumulative lifetime exposure to solar irradiance

Exposure	9 days[a]	16 days[a]	25 days[a]	630 days	631 days
I_{sc} (A)	0.729	0.706	0.708	0.711	0.681
V_{oc} (V)	99.56	97.45	97.70	95.27	96.53
I_{mp} (A)	0.612	0.568	0.590	0.567	0.549
V_{mp} (V)	76.51	74.95	74.22	71.04	73.47
P_{mp} (W)	46.82	42.57	43.82	40.31	40.35

[a]Measured from an identical control module.

6.1 Summary of Results. A summary of the sensitivity analysis is given in Table 8. This table lists the variable ranges that would result in less than a 1% change in maximum power (P_{mp}) RMS modeling errors. A discussion on how to interpret the results in Table 8 follows.

6.2 Analysis and Simplification of Model Inputs. Ground reflectance (ρ_g) did not have a significant effect on model performance if the value was between 0 and 0.7 when the absorbed irradiance is corrected using the measured POA irradiance. The POA irradiance inherently includes the effect of ground reflected irradiance, so when it is used to correct the absorbed irradiance, it removes the model's dependence on ρ_g. If the absorbed irradiance is not corrected with the POA irradiance, then the value used for ρ_g would need to be accurately determined. The range of ground

Table 7 Model parameters calculated from STC data measured from the 2-a-Si technology with progressively longer periods of cumulative lifetime exposure to solar irradiance

Exposure	9 days[a]	16 days[a]	25 days[a]	630 days	631 days
a_{ref} (V)	4.48	4.45	4.44	4.41	4.43
$I_{L,\text{ref}}$ (A)	0.742	0.723	0.723	0.735	0.699
$I_{o,\text{ref}}$ (A)	1.41×10^{-10}	1.77×10^{-10}	1.73×10^{-10}	2.37×10^{-10}	1.94×10^{-10}
$R_{s,\text{ref}}$ (Ω)	16.8	17	18.5	20.9	18.9
$R_{\text{sh,ref}}$ (Ω)	927	686	883	625	712

[a]Calculated from STC data measured from an identical control module.

reflectance without a POA irradiance correction that results in less than a 1% change in P_{mp} RMSE was found to be [0.02–0.14], where 0.1 is the average value for asphalt [14].

The glazing extinction coefficient (K) and the glazing thickness (L), which only occur in the product $K\cdot L$ in the transmittance-absorptance ($\tau\alpha$) equation, did not have a significant effect on the model performance. These model inputs therefore do not need to be determined to a high accuracy; setting $K\cdot L$ to 0 results in less than a 0.4% change in P_{mp} RMSE.

Although the temperature coefficient of short-circuit current ($\alpha_{I_{\text{sc}}}$) is provided by the manufacturers, it has a small effect on model performance and could be set to a value characteristic of the module technology without a significant loss in accuracy. A survey of manufacturer datasheets showed that for a random sampling of four modules each from 17 manufacturers, the range of $\alpha_{I_{\text{sc}}}$ for the mono-Si technologies is [0.0224–0.0900]%/°C with an average of 0.0453%/°C. This range, along with the range found for the poly-Si modules, is within the range determined by the sensitivity analysis that results in less than a 1% change in P_{mp} RMSE. The average of the surveyed mono-Si and poly-Si coefficients (0.049%/°C) would therefore be a good characteristic value for both module technologies.

The range of the glazing refractive indices (n_{glaz}) that resulted in less than a 1% change in P_{mp} RMSE included values characteristic of multiple glazing materials. The range of n_{glaz}, [1.11–3.19], includes the values for the glazing materials of this study's modules and many others. A fixed refractive index of 1.53 for glass is used for all these glazing materials, and the resulting change in P_{mp} RMSE is less than 0.05%.

The range of the material band gap energies ($E_{g,\text{ref}}$) yielding less than a 1% change in P_{mp} RMSE includes values characteristic of multiple cell technologies. The range of $E_{g,\text{ref}}$, [0.88–1.52] eV, includes the values for silicon (1.1 eV), CIS (1.02 eV), copper indium gallium (di)selenide (CIGS) (1.15 eV), cadmium telluride (1.49 eV), gallium arsenide (1.43 eV), and many others [21]. The average of this band gap range, 1.2 eV, could be used for all of these cell technologies and would keep the change in P_{mp} RMSE below 0.9%.

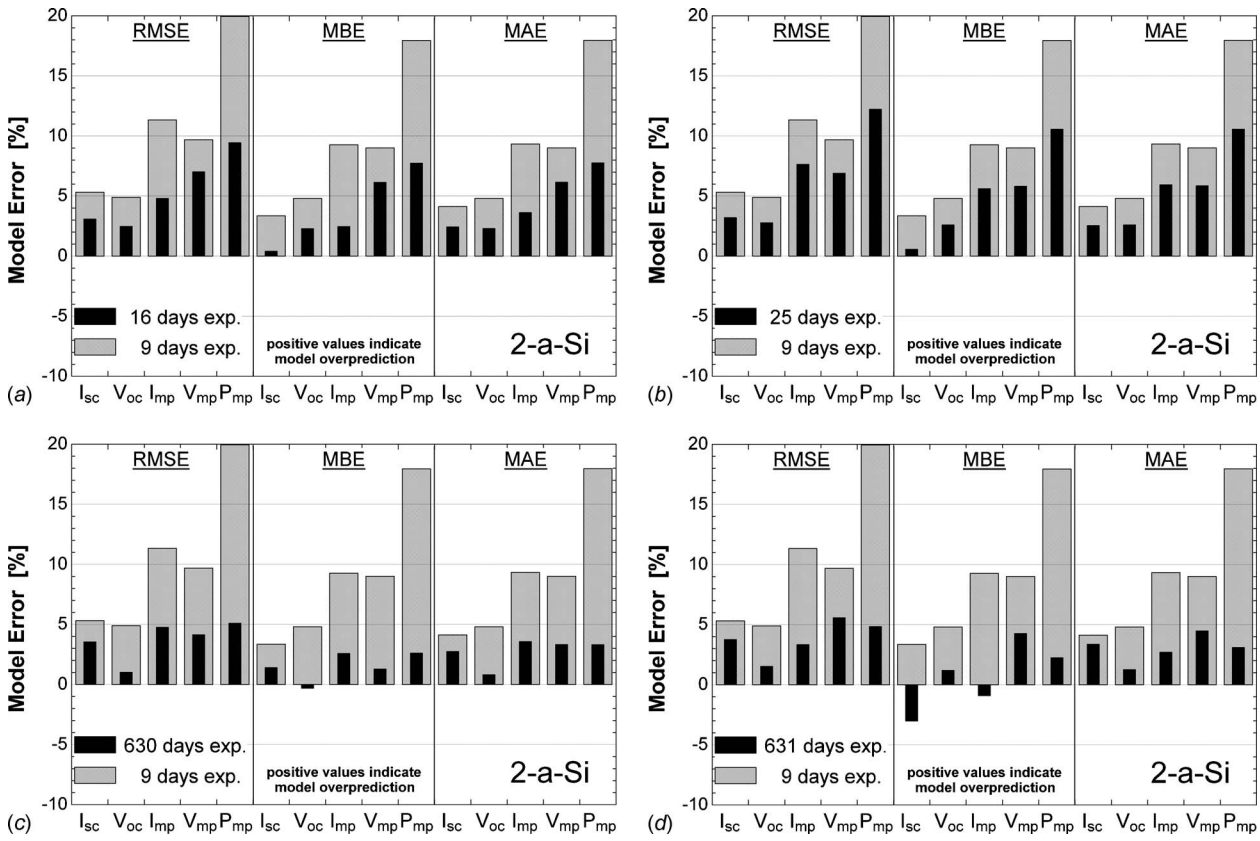

Fig. 7 Statistical modeling errors of the five-parameter model for the 2-a-Si array using the clear days 9:30–4 EST data set and different sets of STC data measured at progressively longer periods of solar exposure

Table 8 Parameter sensitivity in descending order for the five-parameter model using data measured from the mono-Si module in the clear days 9:30–4 EST data set showing the variable ranges that result in less than a 1% change in P_{mp} modeling errors

	Variable	$\leq 1\%$ $\lvert\Delta\text{RMSE}\ P_{mp}\rvert$
Most significant	ΔT_{ref}	[−5.4 K, 4.1 K]
	S_{ref}	[−2.2%, 2.8%]
	$I_{mp,ref}$	[−3.2%, 2.7%]
	$V_{mp,ref}$	[−3.8%, 2.3%]
	$V_{oc,ref}$	[−4.4%, 5.4%]
	$\beta_{V_{oc}}$	[−8.6%, 13%]
	$I_{sc,ref}$	[<−5%, 11.8%]
	$E_{g,ref}$	[−21%, 36%] [0.88 eV, 1.52 eV]
	ρ_g (w/o POA)	[−80%, 40%] [0.02, 0.14]
	n_{glaz}	[−27%, 110%] [1.11, 3.19]
	$\alpha_{I_{sc}}$	[−250%, 150%] [−0.0026 A/C, 0.0044 A/C] [−0.059%/C, 0.10%/C]
	C	[−270%, 480%]
	ΔT_{mod}	[<1 K, >20 K]
	L	[<−100%, 650%] [<0 m, 0.045 m]
	K	[<−100%, 650%]
Least significant	ρ_g (w/POA)	[<−100%, >600%] [<0, >0.7]

6.3 Model Simplification. Using the above characteristic values for ρ_g, $K\cdot L$, $\alpha_{I_{sc}}$, n_{glaz}, and $E_{g,ref}$ and setting C, the temperature dependence of the material band gap, to zero, the change in modeling errors for the four different panels is *less than 0.5% RMSE* for all four of the technologies. However, Fig. 8 shows results from a similar analysis but with $\alpha_{I_{sc}}$ set to zero. It is evident from these results that removing the model's dependence on $\alpha_{I_{sc}}$ by setting it to zero has a significant effect.

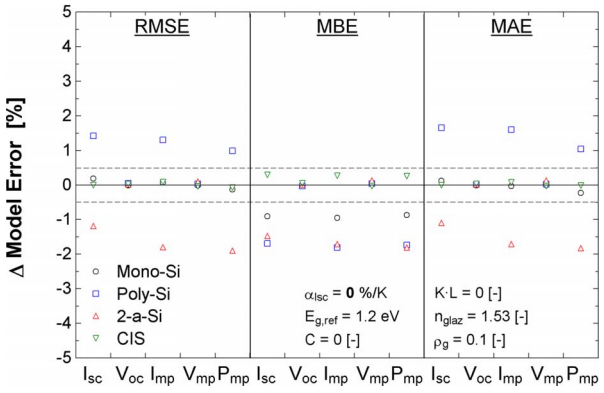

Fig. 8 The change in modeling errors from using accepted values to using characteristic values of $E_{g,ref}$, $K\cdot L$, n_{glaz}, and ρ_g and setting C and $\alpha_{I_{sc}}$ to zero. The modeling errors are calculated for the mono-Si module using the clear days 9:30–4 EST data set.

7 Seven-Parameter Model

The *seven-parameter model* is based on the one-diode equivalent circuit model of a PV cell and is conceptually similar to the five-parameter model. This model is an extension of the six-parameter model, which is currently used by the California Energy Commission (CEC) and is one of the models in the Solar Advisory Model (SAM) developed by NREL. The seven-parameter model uses the same reference parameter values as the five-parameter model but adds two additional parameters that provide temperature and radiation dependence for two of the original parameters [22].

7.1 Additional Model Parameters. The first new parameter is the *nonlinear series resistance temperature dependence*, δ, as given in Eq. (28). The five-parameter model assumes a constant series resistance (R_s).

$$R_s|_T = R_{s,ref} e^{\delta(T-T_{ref})} \tag{28}$$

The temperature coefficient of maximum power (γ) provides the additional information to solve for δ. This temperature coefficient was measured at NIST, but it is also provided by nearly all manufacturers on the module datasheets. The series resistance affects the area of the *I-V* curve nearest to the maximum power point, as shown in Fig. 4(*d*). Both γ and δ provide temperature dependence in this operating region, and they are correlated with R_s by Eqs. (29) and (30) in the seven-parameter model.

$$I_{mp}V_{mp}|_T = P_{mp,ref}(1 + \gamma(T - T_{ref})) \tag{29}$$

$$I_{mp}|_T = I_L - I_o(e^{(V_{mp}+I_{mp}R_s)/a} - 1) - \left.\frac{V_{mp}+I_{mp}R_s}{R_{sh}}\right|_T \tag{30}$$

The second new parameter in the seven-parameter model is the *diode reverse saturation current radiation dependence*, m, as given in Eq. (31). The five-parameter model assumes only temperature dependence for the diode reverse saturation current (I_o). The seven-parameter model adds radiation dependence to this parameter.

$$I_o|_{T,S} = I_{o,ref}\left(\frac{S_{ref}}{S}\right)^m \left(\frac{T}{T_{ref}}\right)^3 \exp\left[\frac{1}{k}\left(\left.\frac{E_g}{T}\right|_{T_{ref}} - \frac{E_g}{T}\right)\right] \tag{31}$$

The maximum power current and voltage at 200 W/m^2 and 25°C provide additional information to solve for parameter m. Although the CEC now requires these data to be provided by manufacturers [23], it was determined in the present analysis by linear regression of approximately 20 operating points nearest to these conditions. The parameter m is determined by fitting the derivative (slope) of the maximum power characteristic equation to zero at 200 W/m^2 and 25°C. This fit is intended to provide better modeling at low irradiance. Model parameters for the mono-Si and 2-a-Si technologies are given in Table 9.

7.2 Model Error. Modeling errors are calculated for the seven-parameter model for the mono-Si and 2-a-Si arrays, which represent the best and worst modeled technologies, respectively, using the five-parameter model. The errors are given in Figs. 9 and 10 for the clear days 9:30–4 EST and January–unshaded pe-

Table 9 Model parameters calculated for the seven-parameter model

Module	a_{ref} (V)	δ (%/°C)	$I_{L,ref}$ (A)	$I_{o,ref}$ (A)	m	$R_{s,ref}$ (Ω)	$R_{sh,ref}$ (Ω)
Mono-Si	1.77	0.460	4.40	1.19×10^{-9}	0.278	1.04	182
2-a-Si (631 day exposure)	4.43	−0.482	0.699	1.94×10^{-10}	1.34	18.9	712

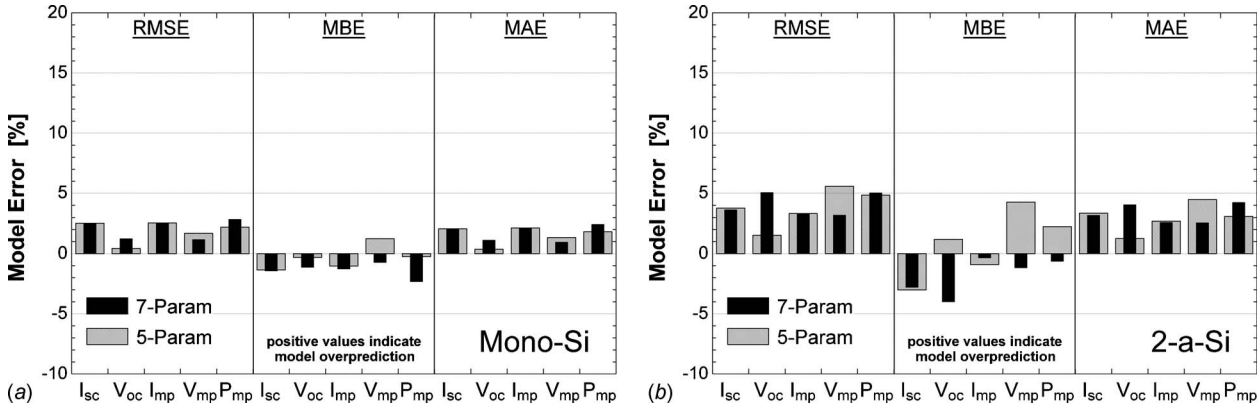

Fig. 9 Five- and seven-parameter modeling errors using the clear days 9:30–4 EST data set for (*a*) mono-Si and (*b*) 2-a-Si technologies

riods data sets, respectively.

Figures 9 and 10 show that the primary differences in predictions between the five- and seven-parameter models are for V_{oc} and V_{mp}. The seven-parameter model exhibits *higher* V_{oc} and *lower* V_{mp} RMS modeling errors as a result of a negative shift in the predicted voltages, as shown by the bias errors. The much lower V_{mp} modeling errors for the January–unshaded periods data set result in approximately 1% lower RMSE for P_{mp}. Additional analysis of these errors is provided in Ref. [17].

The seven-parameter model can be reduced to a six-parameter model by setting either the δ or m parameters to zero because the original five parameters are not dependent on the additional data needed to solve for δ and m. The modeling errors of these two six parameter model variants are calculated for the 2-a-Si array using the January–unshaded periods data set and are given in Fig. 11. These results show that the difference in behavior between the five- and seven-parameter models is caused almost entirely by the addition of the m parameter, with the δ parameter having minimal effect.

A possible explanation of the shift in predicted voltages from the five- to seven-parameter models is found by examining the effect of m on the model, as shown in Fig. 12. Constraining the

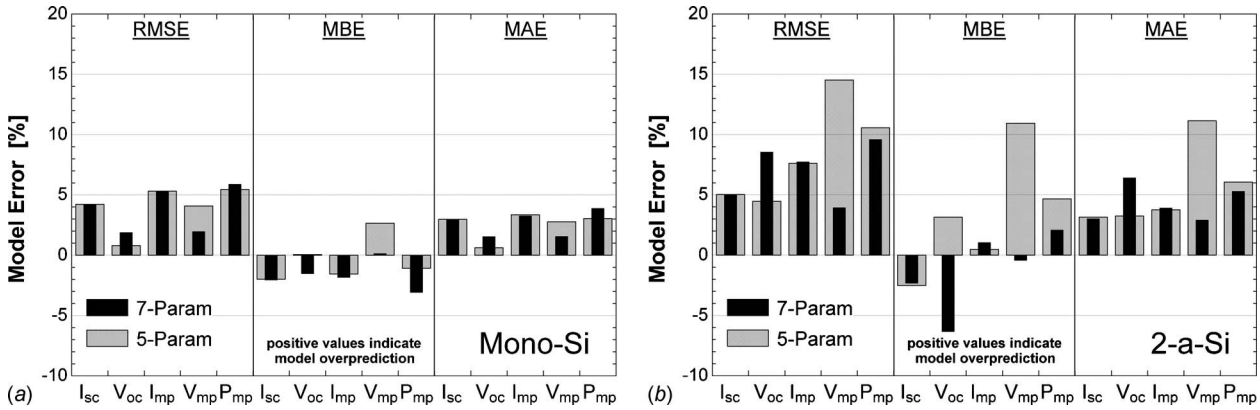

Fig. 10 Five- and seven-parameter modeling errors using the January–unshaded periods data set for (*a*) mono-Si and (*b*) 2-a-Si technologies

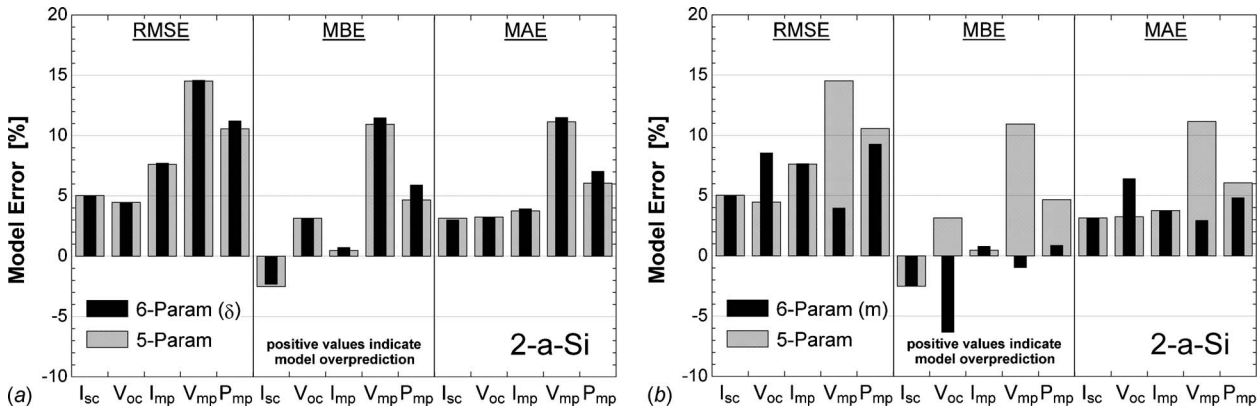

Fig. 11 Five- and six-parameter modeling errors for 2-a-Si using the January–unshaded periods data set. The six-parameter model errors in (*a*) are when $m=0$, while those in (*b*) are when $\delta=0$.

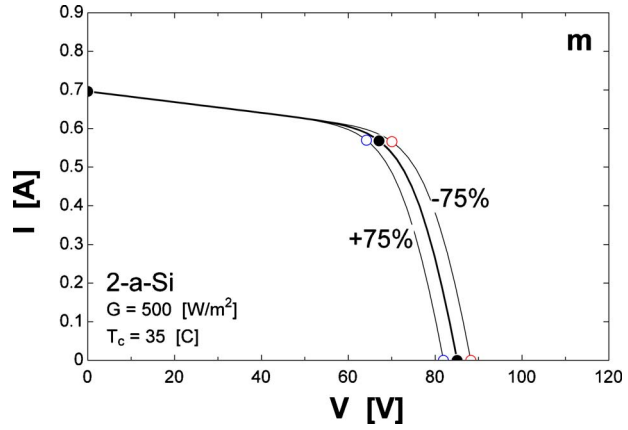

Fig. 12 Effect of parameter *m* in the seven-parameter model on the behavior of the modeled *I-V* curve

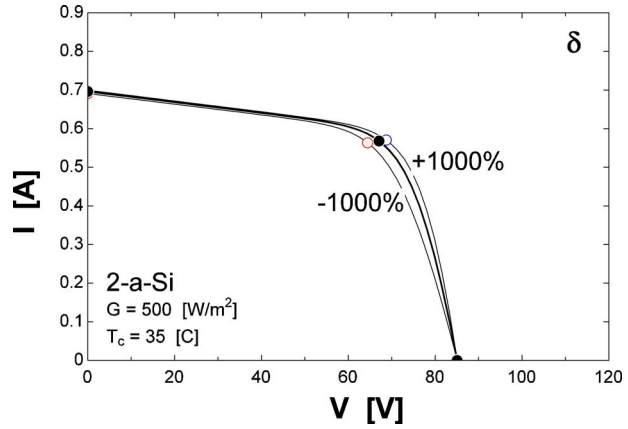

Fig. 13 Effect of parameter δ in the seven-parameter model on the behavior of the modeled *I-V* curve

model at maximum power using the 200 W/m^2 data translates V_{mp}, lowering its respective bias error, but it also translates V_{oc}, increasing its respective bias error. The effect of the second parameter, δ, is shown in Fig. 13, while the effects of the other five parameters are the same as in the five-parameter model, as previously shown in Fig. 4.

8 Recombination Current Differentiation

Previous electrical circuit modeling efforts in this research have used the equivalent circuit shown in solid lines in Fig. 14. A proposed circuit [24] that includes an additional current sink, shown by the dotted lines in Fig. 14, seeks to differentiate the recombination currents in the middle intrinsic layer of an amorphous silicon cell from the currents in the outer semiconductor regions. This intrinsic layer is not present in crystalline silicon cells but is the site of intense recombination in amorphous cells [24]. Recombination currents are modeled in the five-parameter

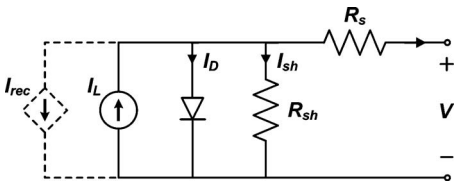

Fig. 14 Equivalent circuit of a photovoltaic solar cell used in the five-parameter model with an added current sink shown in dotted lines

model as a single lumped current through the diode [21] and by the radiation dependence of the shunt resistance and may not accurately capture their separate behaviors.

The additional proposed current sink is defined by Eq. (32); it is dependent on the light current (I_L), the bias voltage ($V+IR_s$), the built-in voltage (V_{bi}), the thickness of the intrinsic layer (d_i), and a new parameter, the $\mu\tau_{eff}$ product. The built-in voltage (V_{bi}) for a module is calculated in this research as the product of the built-in single junction cell voltage (V_c), the number of junctions per cell (N_j), and the number of cells in series (N_s), as given by Eq. (33). The built-in single junction cell voltage (V_c) is 0.9 V for amorphous silicon [25] and approximately 0.6 V for crystalline silicon [21], while N_j is provided by the manufacturer and N_s is either provided by the manufacturer or determined from a visual inspection of the module. The intrinsic layer thickness (d_i) terms and the $\mu\tau_{eff}$ product can be combined into a single new model parameter, designated as chi (χ) in future calculations.

$$I_{rec} = I_L \frac{d_i}{(\mu\tau)_{eff}[V_{bi} - (V + IR_s)]/d_i} \tag{32}$$

$$V_{bi} = V_c N_j N_s \tag{33}$$

8.1 Calculations. The new parameter χ ($d_i^2/\mu\tau_{eff}$) is simultaneously determined along with the original five parameters by constraining the characteristic equation of the new circuit with the maximum power temperature coefficient (γ) at maximum power and a non-reference temperature. The non-reference temperature used in this research is 10 K above the reference temperature, the same temperature difference used to solve for the parameters in the five-parameter model. The equations that relate γ to the model are similar to those in Eqs. (29) and (30) used to solve for δ in the seven-parameter model but use a characteristic equation for the circuit that includes the current sink. This new characteristic equation is defined by Eqs. (34)–(36). The derivative of the characteristic equation is still needed to constrain the model and is provided by Eq. (37). The original constraints for the five-parameter model are used with the maximum power constraint previously described to solve for the six parameters; no temperature or radiation dependence is assumed for χ. Model parameters for the mono-Si and 2-a-Si technologies are given in Table 10.

$$I = I_L - I_{rec} - I_D - I_{sh} \tag{34}$$

Table 10 Model parameters calculated for the six-parameter current sink model

Module	a_{ref} (V)	χ (V)	$I_{L,ref}$ (A)	$I_{o,ref}$ (A)	$R_{s,ref}$ (Ω)	$R_{sh,ref}$ (Ω)
Mono-Si	1.88	0.0285	4.39	4.76×10^{-10}	1.02	214
2-a-Si (631 day exposure)	4.54	6.07	0.727	2.89×10^{-10}	16.7	1920

Note: V_{bi}=43.2 V for the mono-Si module and 122.4 V for the 2-a-Si module.

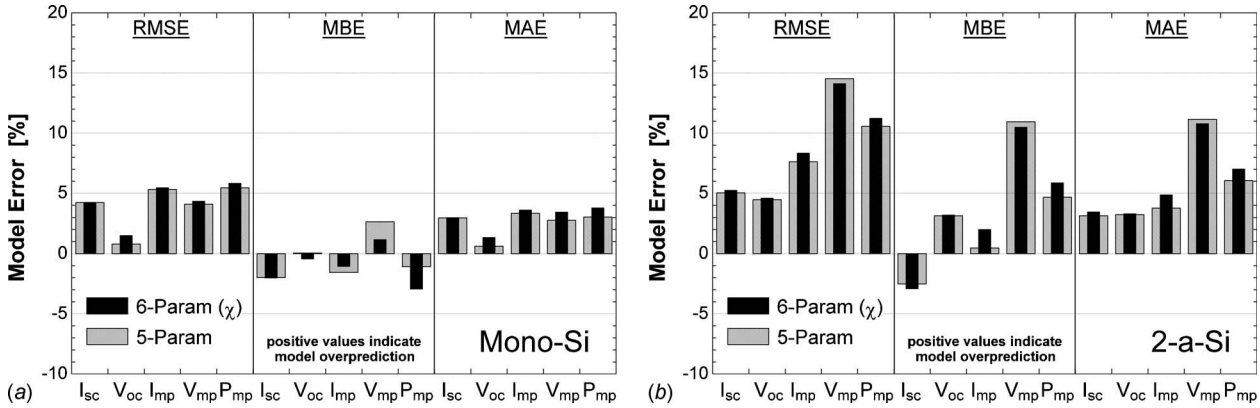

Fig. 15 Six-parameter current sink modeling errors using the January–unshaded periods data set for (*a*) mono-Si and (*b*) 2-a-Si technologies

$$I(V) = I_L - I_L \frac{\chi}{V_{\text{bi}} - (V + IR_s)} - I_o(e^{(V+IR_s)/a} - 1) - \frac{V + IR_s}{R_{\text{sh}}} \tag{35}$$

$$\chi \equiv \frac{d_i^2}{(\mu\tau)_{\text{eff}}} \tag{36}$$

$$\frac{dI}{dV} = \frac{\dfrac{-I_L\chi}{(V_{\text{bi}} - (V + IR_s))^2} - \dfrac{I_o}{a}e^{(V+IR_s)/a} - \dfrac{1}{R_{\text{sh}}}}{1 + \dfrac{I_L\chi R_s}{(V_{\text{bi}} - (V + IR_s))^2} + \dfrac{I_o R_s}{a}e^{(V+IR_s)/a} + \dfrac{R_s}{R_{\text{sh}}}} \tag{37}$$

8.2 Model Error. Modeling errors are calculated for the six-parameter current sink model for the mono-Si and 2-a-Si arrays, the best and worst modeled technologies using the five-parameter model, and are given in Fig. 15 for the January–unshaded periods data set.

It is shown in the above figures that the primary difference in predictions between the five- and six-parameter current sink models occurs at maximum power, with the six-parameter model resulting in 1% higher RMS P_{mp} modeling errors. This effect on the maximum power model predictions is consistent with the effect of χ on the individual *I-V* curves, as shown in Fig. 16.

A sensitivity analysis of the model to V_{bi} was performed using data from the 2-a-Si array that also tested whether the calculated value of this lone new model input provides the best model predictions. The modeling errors were calculated using values for $V_{\text{bi}} \pm 15\%$ of the baseline value; solutions to the model parameters do not converge at larger deviations. Results for the analysis show that the model is rather insensitive to V_{bi}, with only a 0.09% change in P_{mp} RMSE at $V_{\text{bi}}+15\%$ and only a 0.6% change in P_{mp} RMSE at $V_{\text{bi}}-15\%$. The V_{bi} parameter had less of an influence on the other operating points. The higher modeling errors for the six-parameter current sink model relative to the five-parameter model can therefore not be attributed to an uncertainty in V_{bi} and must either be caused by an uncertainty in γ or a deficiency in the model.

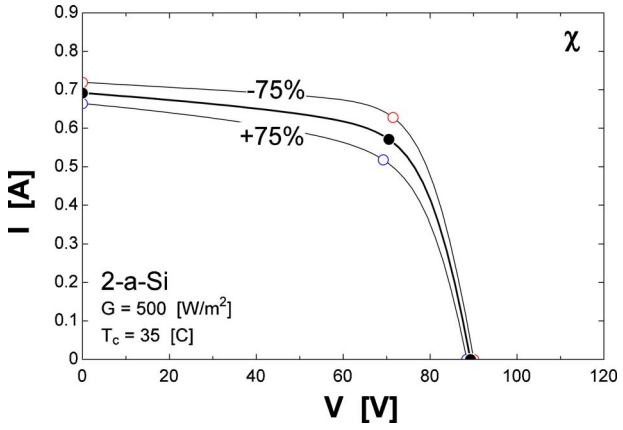

Fig. 16 Effect of the χ parameter in the six-parameter current sink model on the behavior of the modeled *I-V* curve

9 Conclusions

The five-parameter equivalent circuit model accurately predicts the performance of crystalline solar modules under varied operating conditions, but it does not perform as well for amorphous and thin-film technologies. The difference between model-predicted and measured maximum power values for the monocrystalline and polycrystalline silicon modules is approximately 3% and 6% RMS for the clear days and January data sets, respectively, while the differences are about twice as high for CIS (6% and 10%, respectively) and more than four times as high for tandem-junction amorphous (20% and 27%, respectively). The predictions for the amorphous technology can be improved to 5% for the clear days data set and 11% for the January data set if the model parameters are calculated directly from characterization data obtained after the module underwent an initial degradation in output due to aging, which is a characteristic behavior of amorphous silicon. The model predictions for the amorphous technologies are still not as accurate as those for the crystalline technologies, which may be due to unaccounted spectral effects. The spectral distribution of the irradiance has been shown to have a small effect on the performance of crystalline technologies, but it may have a greater effect on the performance of amorphous technologies [7,1]. The model presented in this paper does not account for spectral dependence.

A sensitivity analysis of the five-parameter model shows that a single representative value can be used for all inputs that are difficult to determine or not provided by manufacturer datasheets such as the short-circuit current temperature coefficient, the glazing material properties, the semiconductor band gap energy, and the ground reflectance. The use of these values results in less than a 0.25% RMS change in modeling errors relative to using the accepted values.

Modifications to the five-parameter model evaluated in this paper did not appreciably improve overall model performance. The temperature and radiation dependence introduced by a seven-parameter model had less than a 1% RMS effect on maximum power predictions for the amorphous technology but increased the modeling errors for this array 4% RMS at open-circuit conditions.

Adding a current sink to the equivalent circuit to better account for recombination currents was found to have less than a 1% RMS effect on all characteristic operating points.

Acknowledgment

The authors wish to acknowledge NREL for providing the funding to complete this project and Nate Blair and other researchers at NREL for their helpful feedback. Special thanks to Professor William Beckman in assisting with the seven-parameter model and also to Ty Neises for the simulations and plotting relating to the sensitivity analysis of the five-parameter model.

Nomenclature

A_i = anisotropy index (HDKR model)
a = ideality factor (V)
C = band gap temperature coefficient (%/K)
d_i = thickness of intrinsic layer (m)
E_g = band gap energy (eV)
f = modulating factor (HDKR model)
G = total irradiance on a horizontal surface (W/m^2)
G_b = beam irradiance (W/m^2)
$G_{b,n}$ = beam irradiance normal to a plane (W/m^2)
G_d = diffuse irradiance (W/m^2)
G_{on} = extraterrestrial radiation normal to a plane (W/m^2)
G_T = irradiance on a tilted surface (W/m^2)
I = current (A)
I_D = diode current (A)
I_L = light current (A)
I_{mp} = maximum power current (A)
I_o = diode reverse saturation current (A)
I_{rec} = recombination current (A)
I_{sc} = short-circuit current (A)
I_{sh} = shunt current (A)
K = extinction coefficient (m^{-1})
L = thickness of module glazing (m)
m = diode reverse saturation current radiation dependence
n = refractive index
N_j = number of cell junctions
N_s = number of cells in series
NOCT = nominal operating cell temperature (°C)
P_{mp} = maximum power (W)
POA = plane-of-array
R_b = ratio of beam irradiance on a tilted surface to beam irradiance on a horizontal surface
R_s = series resistance (Ω)
R_{sh} = shunt resistance (Ω)
S_T = absorbed irradiance on a tilted surface (W/m^2)
STC = standard test conditions
T = temperature (°C)
V = voltage (V)
V_{bi} = built-in cell voltage (V)
V_c = built-in single junction cell voltage (V)
V_{mp} = maximum power voltage (V)
V_{oc} = open-circuit voltage (V)
$\alpha_{I_{mp}}$ = maximum power current temperature coefficient (A/°C)
$\alpha_{I_{sc}}$ = short-circuit current temperature coefficient (A/°C)
β = slope of module (deg)
$\beta_{V_{mp}}$ = maximum power voltage temperature coefficient (V/°C)
$\beta_{V_{oc}}$ = open-circuit voltage temperature coefficient (V/°C)
γ = maximum power temperature coefficient (%/K)
δ = nonlinear series resistance temperature dependence (%/°C)
δ_{dec} = declination (deg)
θ = incidence angle (deg)
θ_r = angle of refraction (deg)
$\mu\tau_{eff}$ = effective free carrier mobility (m^2/V)
ρ_g = ground reflectance
$(\tau\alpha)$ = transmittance-absorptance product
φ = latitude (deg)
χ = current-sink parameter (V)
ω = hour angle (deg)

References

[1] De Soto, W., Klein, S. A., and Beckman, W. A., 2006, "Improvement and Validation of a Model for Photovoltaic Array Performance," Sol. Energy, **80**(1), pp. 78–88.
[2] Müllejans, H., Hyvärinen, J., Karila, J., and Dunlop, E., 2004, "Reliability of Routine 2-Diode Model Fitting of PV Modules," Proceedings of the 19th European Photovoltaic Conference, Paris, France.
[3] King, D., Dudley, J., and Boyson, W., 1996, "PVSIM: A Simulation Program for Photovoltaic Cells, Modules, and Arrays," Proceedings of the 25th IEEE Photovoltaic Specialists Conference (PVSC), Washington, DC.
[4] Eikelboom, J., and Reinders, A., 1997, "Determination of the Irradiation Dependent Efficiency of Multicrystalline Si PV Modules on Basis of IV Curve Fitting and Its Influence on the Annual Performance," Proceedings of the 14th European Photovoltaic Solar Energy Conference, Barcelona, Spain.
[5] Kurobe, K., and Matsunami, H., 2005, "New Two-Diode Model for Detailed Analysis of Multicrystalline Silicon Solar Cells," Jpn. J. Appl. Phys., Part 1, **44**(12), pp. 8314–8321.
[6] Duffie, J., and Beckman, W., 2006, *Solar Engineering of Thermal Processes*, 3rd ed., Wiley, New York.
[7] King, D., Boyson, W., and Kratochvill, J., 2004, "Photovoltaic Array Performance Model," Sandia National Laboratories, Report No. SAND2004-3535.
[8] Skoplaki, E., Boudouvis, A., and Palyvos, J., 2008, "A Simple Correlation for the Operating Temperature of Photovoltaic Modules of Arbitrary Mounting," Sol. Energy Mater. Sol. Cells, **92**, pp. 1392–1402.
[9] Del Cueto, J., 2000, "Model for the Thermal Characteristics of Flat-Plate Photovoltaic Modules Deployed at Fixed Tilt," Proceedings of the 28th IEEE PV Specialist Conference (PVSC), Anchorage, AK.
[10] Davis, M. W., Fanney, A. H., and Dougherty, B. P., 2001, "Prediction of Building Integrated Photovoltaic Cell Temperatures," ASME J. Sol. Energy Eng., **123**(3), pp. 200–210.
[11] Fuentes, M., 1987, "A Simplified Thermal Model for Flat-Plate Photovoltaic Arrays," Sandia National Laboratories, Report No. SAND85-0330.
[12] Dougherty, B. P., Fanney, A. H., and Davis, M. W., 2005, "Measured Performance of Building Integrated Photovoltaic Panels—Round 2," ASME J. Sol. Energy Eng., **127**(3), pp. 314–323.
[13] Cameron, C., Boyson, W., and Riley, D., 2008, "Comparison of PV System Performance-Model Predictions With Measured PV System Performance," Proceedings of the 33rd IEEE PV Specialist Conference (PVSC), San Diego, CA.
[14] American Concrete Pavement Association (ACPA), 2002, "AIBEDO: A Measure of Pavement Surface Reflectance," Concrete Pavement Research and Technology Update No. 3.05.
[15] Brandrup, J., Immergut, E. H., and Grulke, E. A., 1999, *Polymer Handbook*, 4th ed., Wiley-Interscience, New York.
[16] DuPont, 2006, "Teflon Films," retrieved from http://www2.dupont.com/Teflon_Industrial/en_US/assets/downloads/k15778.pdf, Jan. 8, 2009.
[17] Boyd, M., 2010, "Evaluation and Validation of Equivalent Circuit Photovoltaic Solar Cell Performance Models," MS thesis, University of Wisconsin Solar Energy Laboratory, Madison, WI.
[18] Stutenbaeumer, U., and Mesfin, B., 1999, "Equivalent Model of Monocrystalline, Polycrystalline and Amorphous Silicon Solar Cells," Renewable Energy, **18**(4), pp. 501–512.
[19] Van Zeghbroeck, B., 2007, "Principles of Semiconductor Devices," retrieved from http://ecee.colorado.edu/~bart/book/book/chapter2/ch2_3.htm, Oct. 12, 2009.
[20] Klein, S. A., 2009, "EES–Engineering Equation Solver," F-Chart Software, http://www.fchart.com
[21] 2003, *Handbook of Photovoltaic Science and Engineering*, A. Luque and S. Hegedus, eds., Wiley, New York.
[22] Beckman, W., 2009, Seven-Parameter Model, Under development at the University of Wisconsin Solar Energy Laboratory (SEL), private communication.
[23] California Energy Commission (CEC), 2008, Guidelines for California's Solar Electric Incentive Programs (Senate Bill 1) Second Edition, CEC-300-2008-007-CMF, State of California Energy Commission.
[24] Merten, J., Asensi, J. M., Voz, C., Shah, A. V., Platz, R., and Andreu, J., 1998, "Improved Equivalent Circuit and Analytical Model for Amorphous Silicon Solar Cells and Modules," IEEE Trans. Electron Devices, **45**(2), pp. 423–429.
[25] Nonomura, S., Okamoto, H., and Hamakawa, Y., 1982, "Determination of the Built-in Potential in a-Si Solar Cells by Means of Electroabsorption Method," Jpn. J. Appl. Phys., Part 2, **21**(8), pp. L464–L466.